Li *et al. Microstructures* **2025**, *5*, 2025075
**DOI:** 10.20517/microstructures.2024.134

**Microstructures**

**Review**

**Open Access**

Check for updates

# Lattice softening in thermoelectric materials

**Chen Li[#], Zihang Zhou[#], Yue Lou, Liangwei Fu**

School of Chemistry and Chemical Engineering, Nanjing University of Science and Technology, 200 Xiaolingwei street, Xuanwu District, Nanjing 210094, Jiangsu, China.
[#]These authors contributed equally to this work.

**Correspondence to:** Yue Lou and Liangwei Fu, School of Chemistry and Chemical Engineering, Nanjing University of Science and Technology, 200 Xiaolingwei street, Xuanwu District, Nanjing 210094, Jiangsu, China. E-mails: louyue@njust.edu.cn; fulw@njust.edu.cn

**How to cite this article:** Li, C.; Zhou, Z.; Lou, Y.; Fu, L. Lattice softening in thermoelectric materials. *Microstructures* **2025**, *5*, 2025075. https://dx.doi.org/10.20517/microstructures.2024.134

**Received:** 25 Nov 2024 **First Decision:** 27 Feb 2025 **Revised:** 11 Mar 2025 **Accepted:** 26 Mar 2025 **Published:** 18 Jun 2025

**Academic Editors:** Jing-Feng Li, Zhigang Chen **Copy Editor:** Shu-Yuan Duan **Production Editor:** Shu-Yuan Duan

## Abstract

Lattice softening refers to reducing the lattice stiffness of materials by weakening the binding force between atoms, thereby changing the electron and phonon transport characteristics. The advantage of lattice softening compared to other strategies for optimizing the properties of thermoelectric materials is that it can significantly reduce the lattice thermal conductivity by reducing the sound velocity without significantly affecting the electrical properties. Moreover, lattice softening shows a wide range of application potential in other material fields, such as magnetostrictive materials and intermetallic alloys. However, systematic reviews on the causes, effects, and specific applications of lattice softening in thermoelectric materials are still limited. This review introduces the recent progress of lattice softening in thermoelectric materials, focusing on how to achieve it and its mechanism in optimizing thermoelectric performance. Through mechanical strain engineering, chemical doping, and phase transition strategies to achieve lattice softening, one could lower the phonon speed, reduce the lattice thermal conductivity, and optimize the Seebeck coefficient and conductivity. In the outlook section, the potential applications of lattice softening in sustainable energy technologies are explored.

**Keywords:** Thermoelectric materials, lattice softening, phonon transport, lattice thermal conductivity

## INTRODUCTION

Since the beginning of the 21st century, the excessive exploitation and consumption of non-renewable

energy sources have intensified the energy crisis. According to the International Energy Agency (IEA), one-third of the world's energy is consumed by manufacturing, and 50% of this energy is emitted in the form of industrial waste heat. 60% of this waste heat can be utilized, but only 30% in China[1]. This inefficiency is further underscored by the fact that only around 30% of thermal energy[2] and 34% of fossil fuel energy is efficiently used, with the remainder released into the atmosphere as ineffective waste heat[3], leading to global warming and other environmental issues. This highlights the urgent need for efficient energy utilization and waste heat recovery. The exploration of novel substances concerning the creation and use of renewable energy sources is now crucial. Over the past few decades, research on thermoelectric (TE) materials has provided essential insights into their potential for sustainable energy applications[4-8], particularly in areas such as waste heat recovery[3,9,10], solar energy utilization[11,12], and thermal sensing[13-15]. TE materials can directly convert thermal energy into electricity, making them promising candidates for addressing environmental problems and the energy crisis[16,17].

The properties of TE materials[18] are measured using a dimensionless thermoelectric figure of merit $ZT = S^2\sigma T/\kappa$, where $S$ is the Seebeck coefficient, $\sigma$ is the electrical conductivity, $T$ is the absolute temperature, and $\kappa$ is the total thermal conductivity, consisting of electron thermal conductivity $\kappa_e$ and lattice thermal conductivity $\kappa_l$. To obtain high $ZT$, TE materials must have high $S$, high $\sigma$, and the lowest possible $\kappa$ value. $\kappa_l$ is related to phonon transport, and represents an inverse relationship between the $S$ and the $\sigma$ related by carrier concentration. Higher Seebeck coefficients occur at lower carrier concentrations, as fewer carriers enhance their response to temperature gradients. However, lower carrier concentration reduces electrical conductivity, while higher conductivity increases electronic thermal conductivity and total thermal conductivity, ultimately lowering $ZT$. Researchers need to optimize these parameters through material design and engineering to achieve excellent thermoelectric performance. Traditional methods for optimizing thermoelectric material performance, such as nanocomposite[19-23] and energy band engineering[24-26], make it possible to modify the parameters. Nanocomposites can introduce many interfaces, enhance phonon scattering, and reduce the lattice thermal conductivity of materials. The advantage of energy band engineering is to improve the electrical conductivity and Seebeck coefficient by adjusting the energy band structure, leading to improved power factor value ($S^2\sigma$). However, these methods often involve parameter coupling, making it difficult to simultaneously optimize electrical and thermal performance.

Among the various optimization strategies, lattice softening has gradually emerged as a practical approach for enhancing thermoelectric performance. Lattice softening[27-32] refers to weakening the binding force between atoms, thereby changing the electron and phonon transport characteristics of the material, which is widely used in the fields of thermoelectric[31,33-35], magnetostrictive materials[36-38] and intermetallic alloys[39,40]. Lattice softening mainly reduces lattice thermal conductivity, thus improving thermoelectric efficiency without directly introducing additional phonon scattering, avoiding a significant impact on electrical performance.

Despite the rapid progress in this research field, there is still a lack of systematic evaluation of the specific applications of lattice softening, particularly regarding how lattice softening changes the thermal and electrical conduction performance of materials. This study aims to fill this gap by evaluating the practical application and mechanisms of lattice softening in various thermoelectric materials [Figure 1]. It provides an in-depth analysis of lattice softening on optimizing the coupled thermoelectric parameters, giving a theoretical foundation and practical reference for the design of high-performance thermoelectric materials.

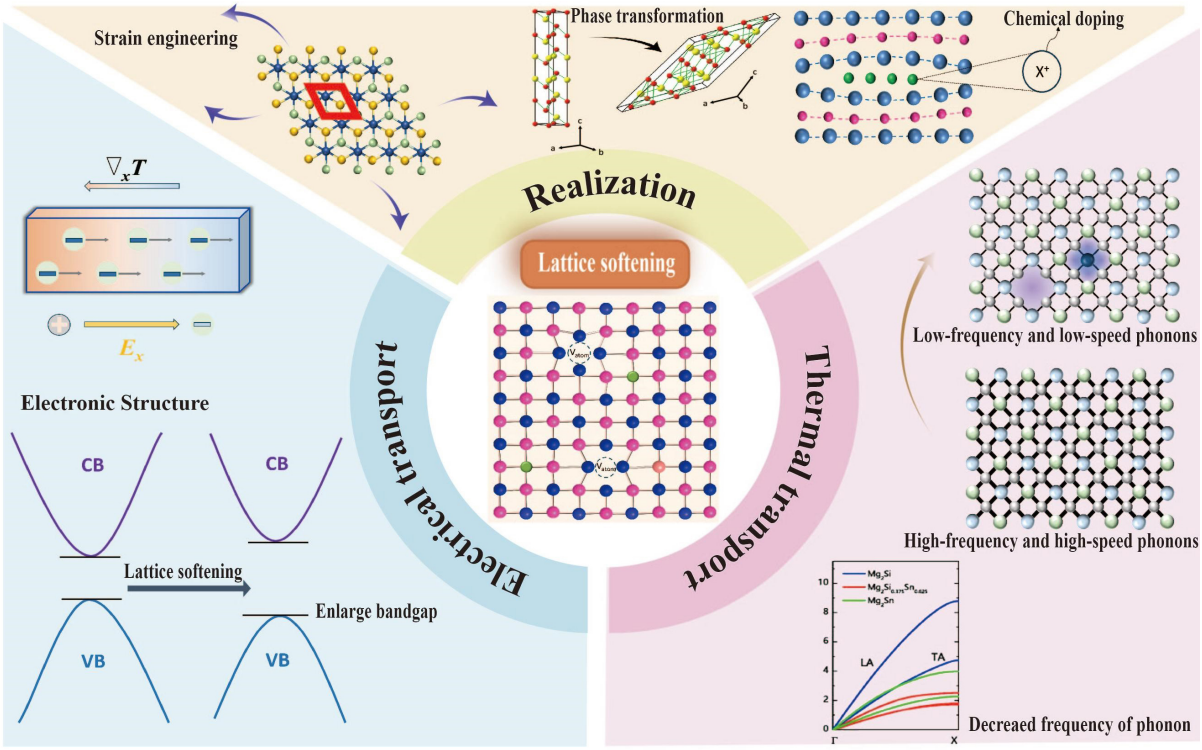


**Figure 1.** The realization of lattice softening and its effect on thermal and electrical properties.

## ADVANTAGES OF LATTICE SOFTENING

Lattice softening changes the physical properties of the thermoelectric material [Table 1]. Its core is to increase lattice constants and weaken the bond strength between atoms. The reduction in bond strength leads to a decrease in the elastic modulus, lattice vibration frequency, and phonon velocity. Lattice softening can be achieved by mechanical strain engineering, chemical doping, and phase transition.

To illustrate the advantages of lattice softening, we minutely contrast it with other traditional strategies for optimizing the properties of thermoelectric materials. Common methods for optimizing the performance of thermoelectric materials include energy band engineering and nanocomposites. Energy band engineering[41] primarily focuses on optimizing electrical performance by modifying the material's band structure, such as band convergence and band flattening. For example, by increasing the band degeneracies, the Seebeck coefficient can be increased without significantly reducing the mobility. As for band flattening, Zhang *et al.*[42] realized that Gd doping flattens the conduction band edge of PbSe, thus resulting in a large Seebeck coefficient. However, its disadvantage is that the energy band structure of the material needs to be accurately adjusted, which puts forward high requirements for the design and synthesis of the material. Nanocomposites means introducing nanostructures into the matrix to optimize thermoelectric properties by nano-effects. The interface between the nanophase and the matrix can strongly scatter phonons, thus significantly reducing the thermal conductivity of the lattice. Bai *et al.*[43] used hydrothermal synthesis to bind functionalized multi-walled carbon nanotubes (f-MWCNTs) into the $Bi_2S_3$ matrix. The enhancement of phonon scattering results in the total thermal conductivity of $Bi_2S_3$/f-MWCNTs nanocomposites at 589 K being 0.27 W $m^{-1}$ $K^{-1}$, which is close to the lowest value of $Bi_2S_3$-based materials. However, the preparation of nanocomposites usually requires precise control of the size, distribution, and interface properties of the nanophase, which places high demands on the synthesis process.

**Table 1. Physical property related to lattice softening in thermoelectric materials**

| Physical property | Description |
|---|---|
| Lattice constant | Increased lattice constant weakens bonding among atoms |
| Elastic modulus | Lower elastic modulus makes lattice softer, affecting thermal and electrical properties |
| Thermal expansion | Lattice softening can directly or indirectly affect the thermal expansion behavior |
| Phonon group speed | Slower phonon speed due to lattice changes further reduces $\kappa_l$ |

Compared to the two methods [Table 2], lattice softening (1) can reduce the thermal conductivity of the lattice more directly while minimizing the negative impact on electrical properties; and (2) does not require complex preparation processes or expensive equipment. This makes the lattice softening strategy suitable for most thermoelectric material systems.

## REALIZATION METHOD OF LATTICE SOFTENING

### Mechanical Strain engineering

Mechanical strain engineering[44-50] is a method of changing the lattice structure of a material by applying mechanical strain. Mechanical strain refers to the deformation of the material under the action of external forces, which can induce lattice softening [Figure 2A].

Hanus *et al.*[28] synthesized stoichiometric PbTe samples under different internal strains induced by high-energy ball milling [Figure 2B]. Bulk PbTe particles with increasing internal strains showed significant phonon velocity reduction (lattice softening). By measuring sonic velocity ($v_s$) and internal strain ($C\epsilon_{XRD}$), a linear relationship was found between the decrease in sound velocity and the increase in the internal strain of the material [Figure 2C], where $\epsilon_{XRD}$ is the internal strain determined via the Williamson-Hall method, and $C$ is a constant related to the nature of the strain and details of the analysis method.

The relationship between strain and phonon frequency (and thus the speed of sound) is described through the Grüneisen tensor

$$\gamma_{ij} = -\frac{d\ln\omega}{d\epsilon_{ij}} \tag{1}$$

which at small strains can be written as

$$\omega = \omega_0\left(1 - \gamma_{ij}\epsilon_{ij}\right) \tag{2}$$

where $\omega_0$ is the phonon frequency at zero strain. Recognizing that $\omega \propto v_s$ at low $\omega$, it is possible to define an engineering Grüneisen parameter $\gamma_{int}$, which is associated with the internal-strain state of PbTe measured via X-ray diffraction (XRD). Then

$$v_s = v_{s,0}(1 - \gamma_{int}\epsilon_{XRD}) \tag{3}$$

This expression is consistent with the experimental observation of a linear dependence of the speed of sound on the strain. From a fit of Equation 3 to the experimental data in Figure 2C using $C = 4$, $\gamma_{int}$ is estimated to be 5, which is similar to the thermodynamic Grüneisen parameter of PbTe.

Huang *et al.*[51] studied the graphene monolayer samples under mechanical stripping by Raman spectroscopy. With uniaxial stress to graphene [Figure 2D], 2D and G bands of graphene were significantly

**Table 2. Advantages and disadvantages of three methods for optimizing the TE performance**

| Method | Advantages | Disadvantages |
|---|---|---|
| Lattice softening | Structural changes lower lattice thermal conductivity | - |
| | Softened lattice enlarges band gap | |
| Band engineering | Band structure modulation increases carrier concentration and mobility | Requires sophisticated growth and doping techniques |
| | | Not all materials are suitable for band engineering |
| Nanocomposites | Interface scattering decreases lattice thermal conductivity | Interfaces in nanocomposites may be unstable |
| | Better mechanical strength | Complex manufacturing processes increase costs |

TE: Thermoelectric.

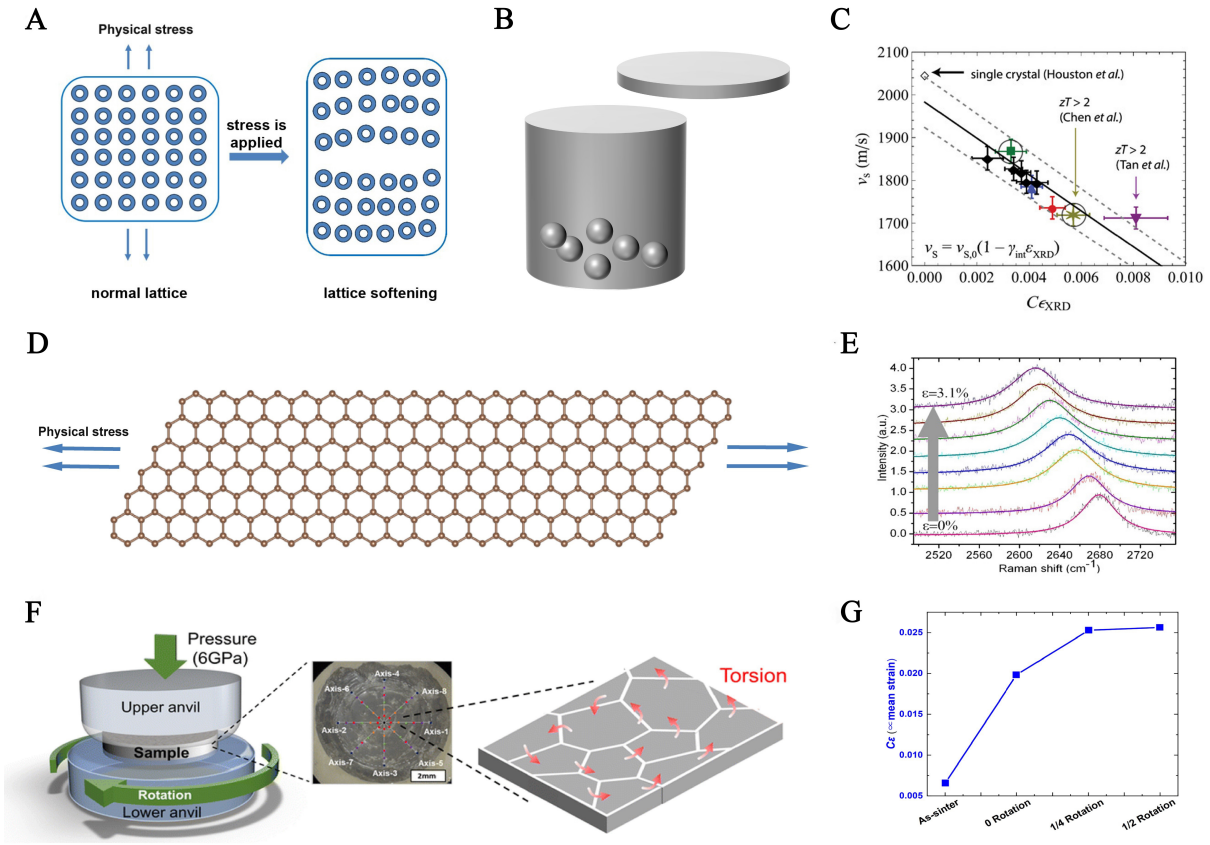


**Figure 2.** (A) Schematic diagram of lattice softening caused by mechanical strain; (B) Schematic diagram of ball milling; (C) The speed of sound ($v_s$) measured by pulse-echo ultrasound versus the internal strain ($C\epsilon_{XRD}$) as measured. Copyright 2019, Wiley[28]. (D) Schematic diagram of graphene tensile test; (E) Evolution of the spectra of the 2D under strain. Copyright 2009, Wiley[51]; (F) Schematic of HPT instrument and method; insert is the picture of the as-processed sample and a schematic of how the stress is introduced; (G) Internal inhomogeneous strain characterization of as-sintered and HPT-processed silicon under 0-1/2 rotation, grain size, and mean strain ($C\varepsilon$) obtained from the analysis. Copyright 2023, Royal Society of Chemistry[52]. XRD: X-ray diffraction; HPT: high-pressure torsion.

redshifted under strain [Figure 2E], which indicates the occurrence of phonon softening. Xu *et al.*[52] applied a moderate high-pressure torsion (HPT) process [Figure 2F] to nanocrystalline silicon by directly introducing finer nanostructures and internal strains, resulting in a global lattice softening and a significant boundary softening effect [Figure 2G], which reduced the phonon group velocity and enhanced phonon scattering at grain boundaries, respectively. A record low $\kappa_l$ of 1.49 W m$^{-1}$ K$^{-1}$ was achieved.

### Chemical doping

Chemical doping[31,53-57] can alter the lattice structure of the material by introducing doping atoms with mismatched dimensions, thus achieving lattice softening [Figure 3A]. For example, Zhang *et al.*[58] chose room-temperature cubic $GeMnTe_2$ as the matrix to alloy Ag and Sb at the Ge/Mn site [Figure 3B]. Due to the huge difference [Figure 3C] in atomic electronegativity, mass, and radius, lattice softening would be caused, thereby reducing sound velocity and resulting in a significant reduction in lattice thermal conductivity. The introduction of certain doping atoms increases the number density of vacancies, which affects the stiffness of the lattice. In previous work, our group[59] modulated the number density of two-dimensional 2D Te vacancies in lead telluride (PbTe) by doping bismuth and indium [Figure 3D]. DFT calculations show that (Bi, In) co-doping reduces the formation energy of these defects, and increases the density of single-atom-layer two-dimensional vacancy ($D_{2D\text{-}vac}$). 2D Te vacancy causes bond softening [Figure 3E], significantly reducing the phonon velocity and lattice thermal conductivity.

Chemical doping can also soften the lattice by affecting the van der Waals bond, metavalent bonding, and bonding (stabilizing) and antibonding (destabilizing) states. Zhu *et al.*[60] investigated the high-temperature thermoelectric properties of $(Bi_2)_m(Bi_2Te_3)_n$ series compounds, revealing multiple mechanisms for their intrinsic low lattice thermal conductivity. $(Bi_2)_m(Bi_2Te_3)_n$ natural superlattice series compounds have layered structures [Figure 3F]. It consists of $Bi_2Te_3$ quintuple layers [Te-Bi-Te-Bi-Te] and a bismuth double layer ($Bi_2$) stacked along the C-axis, with van der Waals bonds between the layers. Compared to $Bi_2Te_3$, the insertion of a bismuth bilayer in the $(Bi_2)_m(Bi_2Te_3)_n$ compound changes the interlayer van der Waals bond action, resulting in reduced longitudinal and transverse sound velocity. The decrease in sound velocity indicates the weakening of the interlayer bond (van der Waals bond). The weakening of the bond has an important effect on the lattice thermal conductivity. The $(Bi_2)_m(Bi_2Te_3)_n$ compound thus has extremely low lattice thermal conductivity [Figure 3G], such as $\kappa_l$ of about 0.42 W $m^{-1}$ $K^{-1}$ for $Bi_8Te_9$ at 300K, much lower than the $\kappa_l$ of $Bi_2Te_3$ at 300 K (about 1.6 W $m^{-1}$ $K^{-1}$). In the field of thermoelectric materials, metavalent bonding[61-65] (MVB), as a unique form of chemical bonding, describes a special semi-filled σ bond with only one electron between adjacent atoms, which is essentially a competition between electron localization and delocalization. Liu *et al.*[66] significantly improved the solid solubility of Ag in SnTe [Figure 3H] by combining with $AgSbTe_2$ compounds with the same metavalent bond [Figure 3I]. Due to atomic size differences and other factors, the doping of Ag will produce lattice strain in the lattice. The related lattice strain softens the phonons and significantly reduces the lattice thermal conductivity, resulting in the lattice thermal conductivity of $Sn_{0.87}Mn_{0.08}Sb_{0.08}Te$-5%$AgSbTe_2$ being as low as 0.30 W $m^{-1}$ $K^{-1}$ at 873 K. Wang *et al.*[67] synthesized $Cu_{1.98-2y}Mn_yS$ and $Cu_{1.98-2x}Mn_xS_{0.985}Se_{0.015}$ series polycrystalline samples by high-temperature melt-annealing combined with hot pressing. The DFT calculation shows that when Mn doping $Cu_2S$, Mn's 3d orbital interacts strongly with S's 3p orbital [Figure 3J], weakens the Cu-S bond [Figure 3K], reduces the transition energy barrier and enthalpy change, and stabilizes the low-temperature cubic phase.

### Phase transformation

Phase transition[67-70] refers to the phenomenon that a material changes from one phase (state) to another under different conditions (such as temperature, pressure, chemical environment, *etc.*), including structural phase transition[71-73], superionic phase transition[74-76], and topological transition[77-80]. It can significantly change the lattice structure of the material, thus affecting the physical properties of the material [Figure 4A].

Structural phase transition refers to the change of the crystal structure of the material, such as changing from a cubic system to a hexagonal system. For example, Wang *et al.*[81] achieved chemical bond softening and structural distortion in Te-free $Bi_{2-x}Sb_xSe_3$ by composition-induced (Sb alloying) structural transition from rhomboid phase to orthorhombic phase [Figure 4B], resulting in significant changes in electron band structure and phonon dispersion. At the same time, phonon softening and lattice disharmony caused by

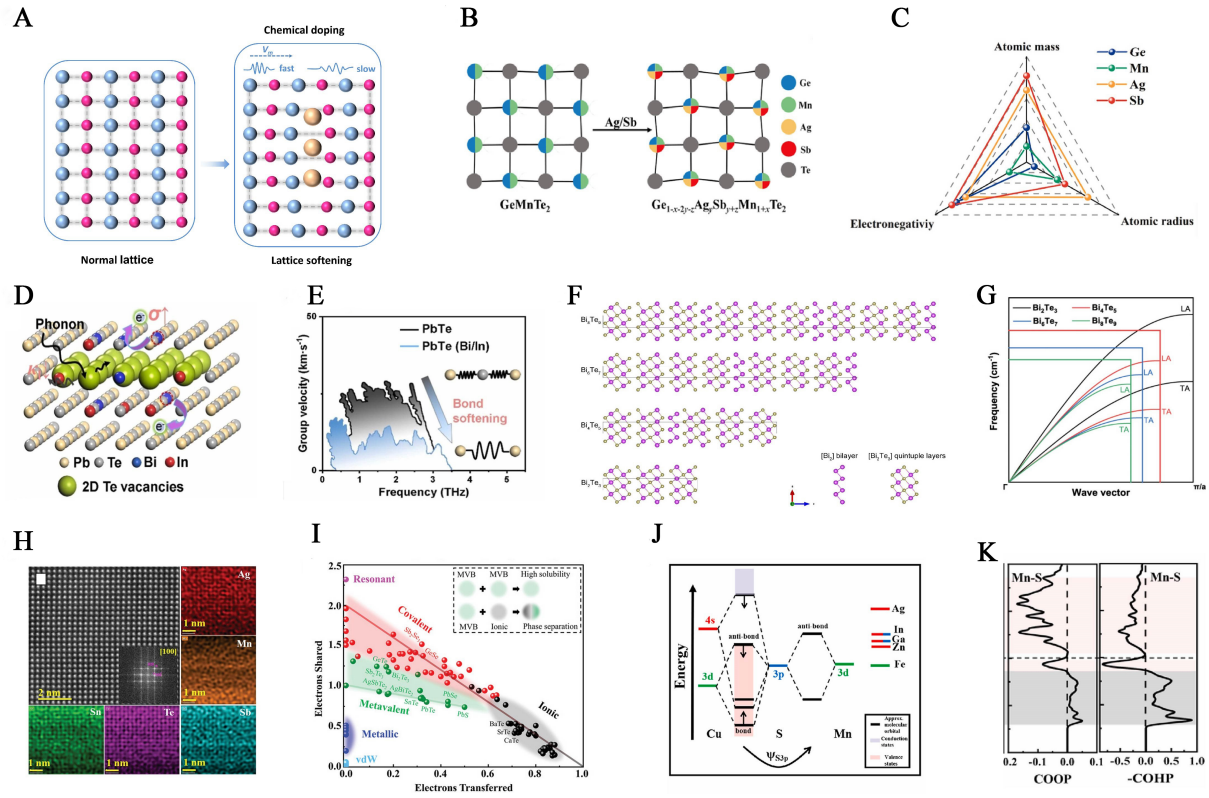


**Figure 3.** (A) Schematic diagram of lattice softening caused by chemical doping; (B) Schematic illustration of lattice anharmonicity due to the complexity of Ge sublattice; (C) Difference between elements (Ge, Mn, Ag and Sb) in atomic mass, radius, and electronegativity. Copyright 2025, Elsevier[58]; (D) Schematic diagram of single-atom-layer 2D Te vacancies, Bi and In doping in $Pb_{0.988}Bi_{0.007}In_{0.005}Te$ crystal structures; (E) Phonon group velocity as a function of frequency for PbTe (black) and PbTe with Bi/In next to 2D vacancy (blue). Copyright 2024, Elsevier[59]; (F) Crystal structure of $Bi_8Te_9$, $Bi_6Te_7$, $Bi_4Te_5$, and $Bi_2Te_3$; (G) A schematic illustration of the underlying mechanisms of the ultralow lattice thermal conductivity in the $(Bi_2)_m(Bi_2Te_3)_n$ (m/n = 3:9, 2:7, and 1:5) homologous series in comparison with $Bi_2Te_3$. The weak chemical bonding leads to low group velocity in the $(Bi_2)_m(Bi_2Te_3)_n$ homologous series compared to $Bi_2Te_3$. In addition, the Brillouin zone of the $(Bi_2)_m(Bi_2Te_3)_n$ homologous series shrinks as the number of atoms in the unit cell increases. Consequently, the high-frequency acoustic phonon modes are cut off because of the low group velocity of the acoustic phonon modes and the small volume of the first Brillouin zone in the $(Bi_2)_m(Bi_2Te_3)_n$ homologous series. Copyright 2021, American Chemical Society[60]; (H) Atomic-resolution HAADF-STEM image of $Sn_{0.87}Mn_{0.08}Sb_{0.08}Te$-5%$AgSbTe_2$ and EDS mappings of SnTe matrix (FFT image that corresponds to the HAADF-STEM image inset); (I) 2D map describing chemical bonds in solids. The map is spanned by the number of electrons transferred normalized by the oxidation state and electrons shared between adjacent atoms. Different chemical bonding mechanisms are demarcated by different colors. Copyright 2022, the Authors. Advanced Functional Materials published by Wiley-VCH GmbH[66]; (J) A schematic band diagram from simple chemical bonding (hybridization) arguments. The schematics of atomic orbital energies of Cu, S, Mn, Ag, In, Ga, Zn, Fe, and the molecular orbital energies of Mn-doped $Cu_2S$ and (K) Mn-doped $Cu_2S$ with hexagonal structures. The bonding (stabilizing) and antibonding (destabilizing) states could be well defined by the COHP values. The bonding orbital (grey area) has negative COHP. Copyright 2023, Elsevier[67]. HAADF-STEM: High-angle annular dark field-scanning transmission electron microscopy; FFT: fast Fourier transformation; EDS: energy dispersive spectrometer; COHP: crystal orbital hamilton populations.

weak interchain interactions greatly hinder the heat-carrying phonons, resulting in a significant decrease in lattice thermal conductivity at 300 K [Figure 4C]. Yang *et al.*[82] quantitatively investigated the relationship between subtle changes in the statically disordered atoms across different CuTeI phases and $\kappa_l$ during phase transitions. Specifically, $\alpha$-CuTeI [Figure 4D] exhibits substantial lattice softening compared to $\beta$-CuTeI [Figure 4E], characterized by a 10.4% decrease in the $v_s$ and a ≈ 2 GPa reduction in the shear modulus at 273 K. The more significant reductions [Figure 4F] in $v_T$ compared to $v_L$ resulted in an increase in the average Grüneisen parameter, which further contributed to a more than 44% reduction in $\kappa_l$.

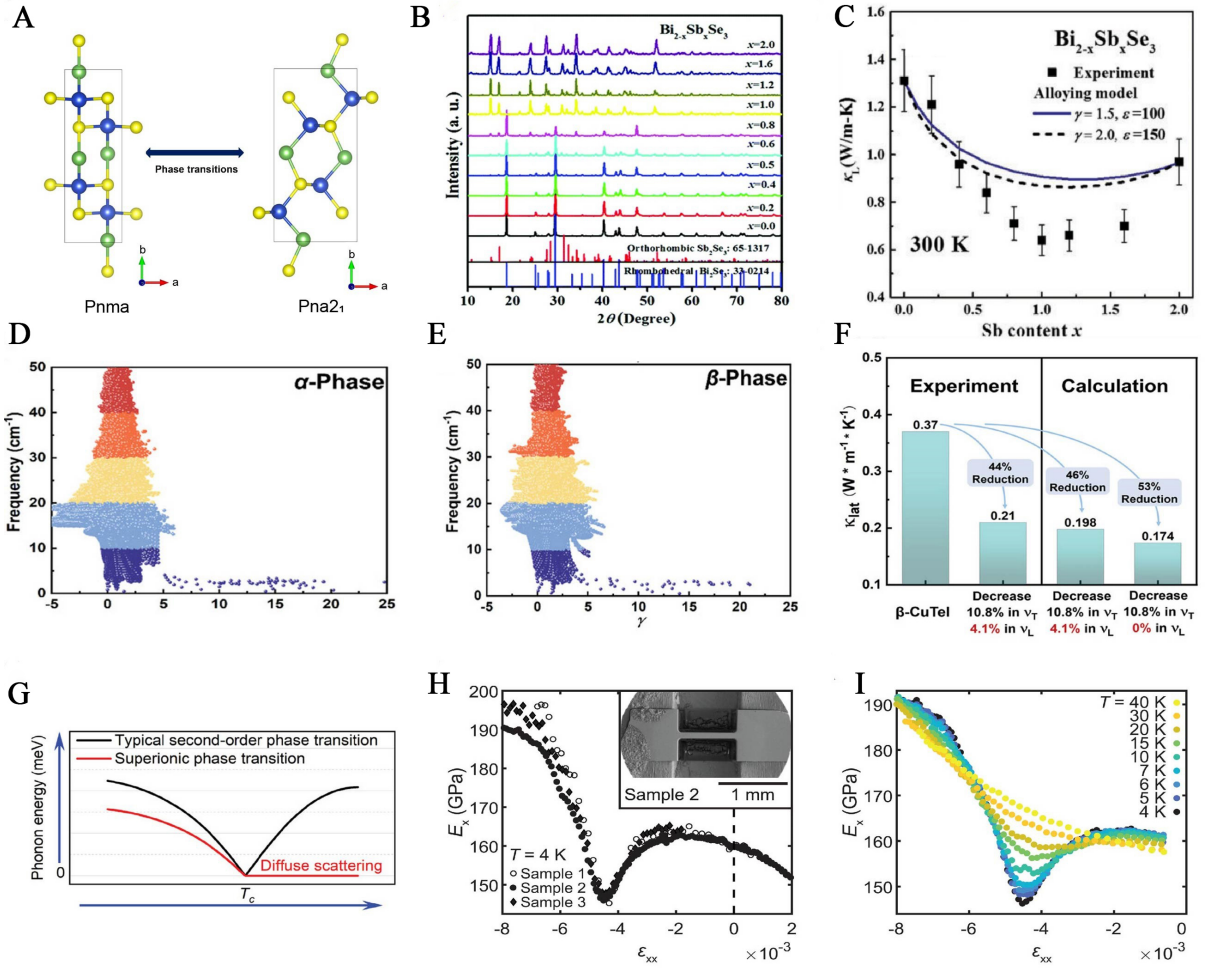


**Figure 4.** (A) Schematic diagram of lattice softening caused by phase transition; (B) Powder XRD patterns for $Bi_{2-x}Sb_xSe_3$; (C) Lattice thermal conductivity as a function of the Sb content for $Bi_{2-x}Sb_xSe_3$. The solid and dashed lines are estimated based on the Klemens-Callaway theory, using different $\varepsilon$ values. Copyright 2016, Royal Society of Chemistry[81]; (D) Grüneisen parameter of $\beta$-phase; (E) Grüneisen parameter of $\alpha$-phase; (F) Experimental and calculated reduction of $\kappa_{lat}$ due to reduced speed of sound. Copyright 2024, Wiley[82]; (G) (Black solid line) Schematic diagram of the temperature dependence of the energy of a typical soft phonon in a second-order phase transition, such as a ferroelectric one. (Red solid line) Soft phonon behavior observed in $Ag_8GeSe_6$ undergoing a superionic phase transition upon heating. Copyright 2023, the Authors. *Small* published by Wiley VCH GmbH[84]; (H) $E_x$ as a function of strain $\varepsilon_{xx}$ measured at 4 K on three samples. Inset: Scanning electron micrograph of sample 2; (I) $E_x$ versus $\varepsilon_{xx}$ at a series of temperatures measured on sample 2. Copyright 2023, AAAS[89]. XRD: X-ray diffraction.

The superionic phase transition[83] refers to the phase transition process in which the mobility of ions in the lattice of the material is significantly increased under certain conditions, resulting in a substantial increase in the conductivity of the material. Shen *et al.*[84] study the case of a superionic phase transition in the Argyrodite $Ag_8GeSe_6$, where the soft mode does not freeze into a static distortion but rather triggers solid state diffusion upon crossing $T_c$. Consistently, no phonon hardening is observed in the superionic phase above $T_c$, and the soft mode maintains its over-damped character, as indicated in Figure 4G.

Two types of topological phase transition that can cause lattice softening are introduced here. Lifshitz phase transition[85-88] is a special topological Fermi surface transition, which occurs when the topological structure of the Fermi surface of the material changes and Fermi levels pass through the Van Hove singularity (VHS), resulting in a change in the density of the electronic states. Noad *et al.*[89] took an ultra-clean, quasi-two-

dimensional correlated metal $Sr_2RuO_4$ single crystal, machined it into a neck and embedded it in an epoxy resin, and used custom equipment to synchronously monitor uniaxial stress and strain. They measured Young's modulus. It is found that at Lifshitz transition strain, Young's modulus decreases significantly [Figure 4H and I], lattice softening reaches 10-15%, and the softening degree increases with decreasing temperature. Another typical topological phase transition is the charge-density-wave (CDW) phase transition[80], which is caused by the interaction between the electron-phonon coupling and the Fermi surface topology, and it causes phonon softening.

## LATTICE SOFTENING AFFECTS ELECTRICAL TRANSPORT PROPERTIES

The electrical transport properties of thermoelectric materials include the conductivity and Seebeck coefficient. Conductivity is a parameter that measures the conductivity of a material, which is related to the carrier concentration and mobility within the material. The Seebeck coefficient describes the ability of a material to generate an electromotive force under temperature difference, which is related to the electronic structure of the material. The corresponding formula is as follows[18]:

$$\sigma = ne\mu \tag{4}$$

$$S = \frac{8\pi^2 k_B^2}{3eh^2} m^* T \left(\frac{\pi}{3n}\right)^{\frac{2}{3}} \tag{5}$$

where $n$, $e$, $\mu$, $h$, $k_B$, and $m^*$ stand for the carrier concentration, elementary charge, carrier mobility, Planck constant, Boltzmann constant, and carrier effective mass, respectively.

Lattice softening caused by chemical doping leads to increased vacancy density, thereby increasing the concentration of carriers and further optimizing the conductivity. Lattice softening can also lead to changes in the band structure [Figure 5A], which can affect the position of the Fermi level and the concentration of carriers.

Zhang *et al.*[90]'s strategy of eliminating p-d hybridization by Ag substitution can achieve a high average $ZT$ in $Cu_3SbSe_4$. Using density functional theory (DFT), it is proved that the weakening of Cu-Se bonds favors the formation of Cu vacancies, which increases carrier concentration and thus reduces resistivity [Figure 5B and C]. Liang *et al.*[91] prepared $Mg_{3.2-x}Mn_xSb_{1.5}Bi_{0.49}Se_{0.01}$ Zintl compounds co-doped with Se and Mn, in which Mn was doped at the Mg site. Since the electronegativity of Mn (1.55) is larger than that of Mg (1.31), the chemical bonds in Mn-doped samples are softened, leading to a significant increase in carrier concentration and mobility. As can be seen from Equation 5, the Seebeck coefficient is inversely proportional to the carrier concentration $S \sim n^{-2/3}$. Therefore, at low temperatures (below 400 K), the Seebeck coefficient of the manganese-doped sample is significantly lower than that of the non-manganese sample. For example, at 323 K, it decreases from -284 μV $K^{-1}$ in the Mn-free sample ($3.92 \times 10^{19}$ $cm^{-3}$) to -250 μV $K^{-1}$ in the x = 0.02 sample ($4.7 \times 10^{19}$ $cm^{-3}$). Tang *et al.*[92] investigated the effect of strain engineering on the thermoelectric properties of asymmetric Janus 1T-SnSSe monolith. Figure 5D presents the top and side views of the 1T-SnSSe monolith, which is formed by the S-Sn-Se covalent bond. The band gap of 1T-SnSSe monolayers increases first and then decreases with the increasing biaxial tensile strain [Figure 5E]. The softened lattice structure (such as the increase in lattice constant) caused by strain is one of the reasons for the change in the band gap, leading to an increase in the Seebeck coefficient. At 300 K, the Seebeck coefficient is 94.60 μV $K^{-1}$ at 0% strain and increases to 189.03 μV $K^{-1}$ at 8% strain. At 900 K, the Seebeck coefficient is 213.37 μV $K^{-1}$ at 0% strain and rises to 214.84 μV $K^{-1}$ at 6% strain.

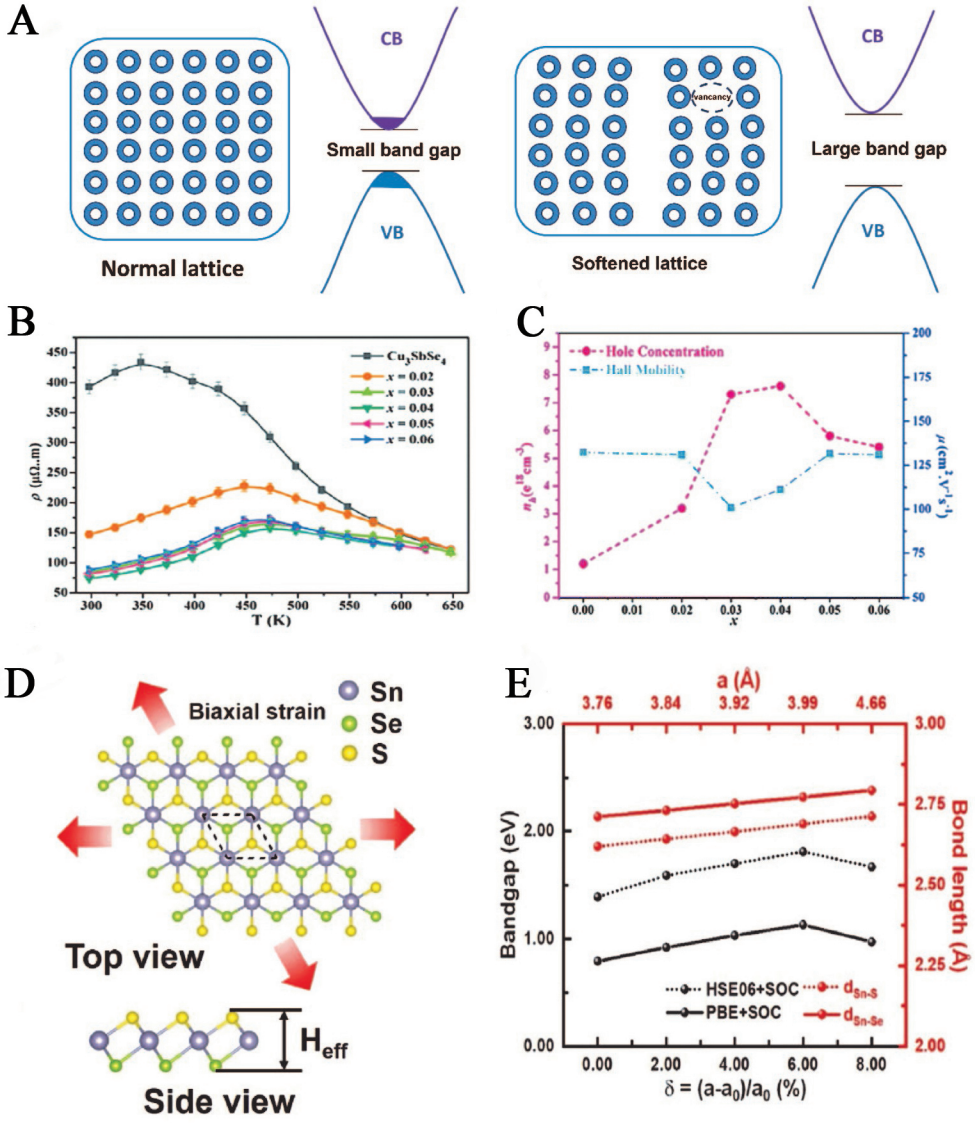


**Figure 5.** (A) Schematic diagram of the effect of lattice softening on electrical transport properties of thermoelectric materials; (B) Temperature-dependent electrical transport properties for $Cu_{3-3x}Ag_{3x}SbSe_4$ (x = 0, 0.02, 0.03, 0.04, 0.05, 0.06) samples: electrical resistivity; (C) Room temperature carrier concentration $n_h$ and carrier mobility $\mu$ as a function of the Ag doping content. Copyright 2019, Royal Society of Chemistry[90]; (D) Top and side views of the crystal structure of 1T-SnSSe monolayer. The Heff in the side view represents the effective thickness of the 1T-SnSSe monolayer; (E) The calculated bandgaps (including the HSE06 + SOC and PBE + SOC methods) as a function of biaxial tensile strains ranging from 0% to 8% and the calculated Sn-S/Sn-Se bond lengths versus the lattice parameters corresponding to the biaxial tensile strains. Copyright 2022, Elsevier[92]. HSE06: Heyd-scuseria-ernzerhof; SOC: spin-orbital coupling effect; PBE: perdew-burke-ernzerhof.

## LATTICE SOFTENING AFFECTS THERMAL TRANSPORT PROPERTIES

The heat conduction of thermoelectric materials mainly includes the contribution of carrier and lattice vibration. Carrier thermal transport is closely related to electric transport, while lattice thermal transport involves phonon propagation. The effect of lattice softening on the lattice thermal conductivity ($\kappa_l$) is reviewed in detail below.

Assuming that phonon-phonon scattering dominates at temperatures well above the Debye temperature, the phonon group velocity ($v_g$) is directly connected to $\kappa_l$, as shown by Equation 6[82]:

$$\kappa_l = \frac{(6\pi^2)^{2/3}}{4\pi^2}\frac{\bar{M}}{(V)^{2/3}T}\frac{\langle v_g^3\rangle}{\gamma^2} \tag{6}$$

where $\bar{M}$ is the average atomic mass, $V$ is the average atomic volume, and $\gamma$ is the Grüneisen parameter. σ is Poisson's ratio, which can be calculated from the ratio of longitudinal to transverse speed of sound ($v_L$/$v_T$). The average frequency-dependent phonon group velocity $v_g$ is approximated as $v_s$, which is identical to the group velocity at the Γ point in the Brillouin zone. The average $v_s$ and $\gamma$ can be calculated according to Equations 7 and 8, respectively[82]:

$$v_s = \left(\frac{1}{3}\left[\frac{1}{v_L^3} + \frac{2}{v_T^3}\right]\right)^{-1/3} \tag{7}$$

$$\gamma = \frac{3}{2}\frac{1+\sigma}{2-3\sigma} \tag{8}$$

In Yang *et al.*'s study[82], they derived Equation 9 based on Equations 6-8:

$$\kappa_l = \frac{(6\pi^2)^{\frac{2}{3}}}{4\pi^2} * \frac{\bar{M}}{(V)^{\frac{2}{3}}T} * \frac{\left(\left(\frac{1}{3}\left[\frac{1}{v_L^3} + \frac{2}{v_T^3}\right]\right)^{-1/3}\right)^3}{\left(\frac{9v_L^2 - 12v_T^2}{2v_L^2 + 4v_T^2}\right)^2} = \frac{A}{\left(\frac{1}{v_L^3} + \frac{2}{v_T^3}\right) * \left(\frac{9v_L^2 - 12v_T^2}{2v_L^2 + 4v_T^2}\right)^2} \tag{9}$$

The right part of the denominator in Equation 9, enclosed in parentheses, is related to the $v_s$, while the left part is associated with the $\gamma$. Importantly, as the variables $\bar{M}$ and V remain relatively constant across different phases at a given temperature, the numerator A can be considered a constant. Consequently, it becomes evident that the variation in $\kappa_l$ can be exclusively linked to the $v_L$ and $v_T$.

Lattice softening decreases the speed of sound ($v_L$ and $v_T$) and elastic modulus [Table 3], thus reducing $\kappa_l$. Most importantly, the softening of the material lattice can achieve the reduced thermal conductivity of the lattice without introducing additional phonon scattering mechanisms. Moreover, lattice softening also significantly increases the thermal expansion rate of materials by changing the lattice spacing and reducing the lattice rigidity.

### Group velocity and frequency of phonons

Phonon group velocity[93-96] is a physical quantity that describes the speed at which phonons (the quanta of lattice vibrations) propagate through a material. The group velocity is closely related to the dispersion relation of phonons, which can be obtained by derivation of the dispersion relation. Specifically, the group velocity of phonons can be calculated by the following formula[95]:

$$v_g = \frac{d\omega}{dq} = \sqrt{\frac{C}{\rho}} \tag{10}$$

where $\omega$ is the frequency of the phonon, $q$ is the wave vector of the phonon, $C$ is the elastic constant (Young's modulus, shear modulus, or bulk elastic modulus) and $\rho$ is the density of the material.

Research on the reduction of lattice thermal conductivity due to lattice softening is prevalent in the field of thermoelectrics. Jiang *et al.*[97] studied the mechanism of electron and phonon localization and found that the crystal symmetry of high-entropy materials improves the electron delocalization distribution

**Table 3. Speed of sound and elastic properties of pristine and doped compounds**

| Compound | Longitudinal/km $s^{-1}$ | Transverse/km $s^{-1}$ | Bulk/GPa | Shear/GPa | Young/GPa |
|---|---|---|---|---|---|
| GeTe | 3.445 | 1.965 | - | - | - |
| $Ge_{0.8}Sn_{0.2}Te$ | 3.365 | 1.833 | - | - | - |
| $Ge_{0.6}Sn_{0.4}Te$ | 3.179 | 1.632 | - | - | - |
| $Ge_{0.4}Sn_{0.6}Te$ | 2.953 | 1.535 | - | - | - |
| $Ge_{0.2}Sn_{0.8}Te$ | 3.331 | 1.876 | - | - | - |
| SnTe | 3.408 | 1.873 | - | - | - |
| $CuGaTe_2$ | 3.84 | 2.08 | 53.1 | 25.4 | 65.8 |
| $Cu_{0.95}Li_{0.05}GaTe_2$ | 3.77 | 2.05 | 50.0 | 24.4 | 63.1 |
| $CuGaTe_{1.99}Sb_{0.01}$ | 3.82 | 2.09 | 51.4 | 25.6 | 65.8 |
| $Cu_{0.05}Li_{0.05}GaTe_{1.99}Sb_{0.01}$ | 3.40 | 1.91 | 37.4 | 20.3 | 51.7 |
| $Cu_{0.95}Ag_{0.05}InTe_2$ | 3.78 | 2.05 | 51.7 | 24.9 | 64.4 |
| $Cu_{0.9}Li_{0.05}Ag_{0.05}InTe_2$ | 3.44 | 1.81 | 43.8 | 19.3 | 50.5 |
| SrCuSb | 4.237 | 2.500 | - | - | - |
| SrAgSb | 3.803 | 2.236 | - | - | - |
| $Sr_2ZnSb_2$ | 3.767 | 2.174 | - | - | - |

[Figure 6A], optimizes the band structure, and improves the electrical properties. At the same time, the disordered distribution of elements produces lattice strain, destroys crystal symmetry, and affects phonons. Raman spectroscopy [Figure 6B] shows phonon mode splitting and transverse phonons are more affected by disorder; sound velocity measurements [Figure 6C] show that the transverse sound velocity $v_t$ drops faster than the longitudinal sound velocity $v_l$, that is, phonon softening, which enhances the anharmonicity, significantly reduces the lattice thermal conductivity, and synergies with electron delocalization to optimize the thermoelectric properties. Han *et al.*[98] found that a 65% reduction in lattice thermal conductivity can be achieved with only 10% covalent Hf doping in a high-band NbFeSb system, compared to the fourfold higher isoelectronic Ta alloying concentration. Figure 6D shows the neutron-weighted phonon DOSs of $Nb_{0.9}X_{0.1}$ FeSb at 5 K. Three phonon bands of 0-20 MeV, 20-30 MeV, and 30-45 MeV were observed, corresponding to one and two phonon bands, respectively. In the energy range of 30-35 MeV, significant softening of optical phonons was observed in Hf- and Zr-doped $Nb_{0.9}Hf_{0.1}FeSb$ and $Nb_{0.9}Zr_{0.1}FeSb$, respectively. Softening of the phonon spectrum means that phonons have lower energies, which can lead to a decrease in the mean free path of phonons. Hanus *et al.*[28] found that lattice softening can significantly reduce thermal conductivity [Figure 6E]. The inset of Figure 6E shows the sound velocity reduction data of different samples; for example, the sound velocity of (Na,Sr)-PbTe is 1860 m $s^{-1}$, and the sound velocity of (Na,Eu)-PbTe is 1719 m $s^{-1}$. The decrease in sound velocity correlates with lattice softening. According to $\kappa_l = A v_s^3 T^{-1}$, a decrease in sound velocity leads to a decrease in $\kappa_l$. The highlighted region in Figure 6E represents the part of reduced $\kappa_l$ caused by lattice softening only, which is obviously different from the part caused by an increase in the phonon-defect scattering center. Tang *et al.*[92] used density functional theory (DFT) and semi-classical Boltzmann transfer theory to study the effect of strain engineering on the thermoelectric properties of asymmetric Janus 1T-SnSSe monolides. As the biaxial tensile strain increases, the lattice thermal conductivity decreases significantly [Figure 6F]. For example, because of lattice softening, the thermal conductivity at room temperature of an unstrained 1T-SnSSe monolellar lattice is about 19.77 W $m^{-1}$ $K^{-1}$, and when a biaxial tensile strain of 8% is applied, the lattice thermal conductivity drops sharply to about 3.53 W $m^{-1}$ $K^{-1}$. Tan *et al.*[99] studied the phonon transport and thermal conductivity of $Mg_2Si_{1-x}Sn_x$ solid solution by first-principles calculation and phonon Boltzmann transport equation. Compared with $Mg_2Si$ and $Mg_2Sn$, the acoustic phonon branch along the direction of "Γ-X" of $Mg_2Si_{0.375}Sn_{0.625}$ was significantly softened [Figure 6G-J]. The acoustic phonon of $Mg_2Si_{0.375}Sn_{0.625}$ has a relatively lower frequency under the same wave vector, which means that the energy of the phonon is reduced and the propagation speed is slowed down, which is a typical representation of lattice softening.

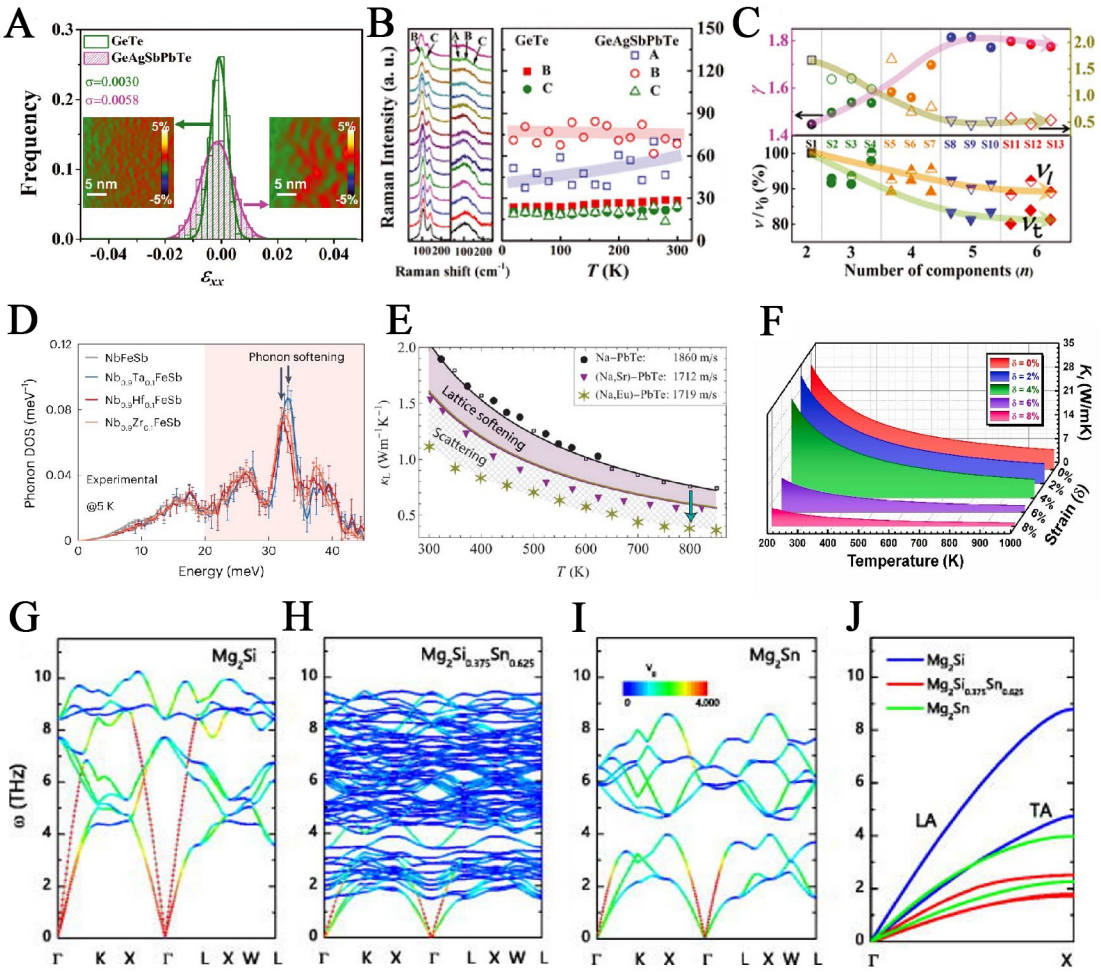


**Figure 6.** (A) Distribution of normal strains in the GeTe and high-entropy $Ge_{0.61}Ag_{0.11}Sb_{0.13}Pb_{0.12}Bi_{0.01}Te$ samples. Left images and green lines are from GeTe samples, and right images and pink lines are from the $Ge_{0.61}Ag_{0.11}Sb_{0.13}Pb_{0.12}Bi_{0.01}Te$ sample. The value of σ is the root mean square; (B) Raman intensity and FWHM of the GeTe (left) and high-entropy $Ge_{0.61}Ag_{0.11}Sb_{0.13}Pb_{0.12}Bi_{0.01}Te$ (middle) samples; (C) Measured sound velocities of the transverse ($v_t$) and longitudinal ($v_l$) waves and the calculated Grüneisen parameter ($\gamma$) and lattice thermal conductivity ($\kappa_l$) values at room temperature, where $v_0$ is the measured sound velocity of the GeTe sample. Copyright 2022, AAAS[97]; (D) Measured neutron-weighted phonon DOSs of the $Nb_{0.9}X_{0.1}FeSb$ compounds. The error bars represent one standard deviation from counting statistics. Copyright 2023, Han *et al.*[98]; (E) A reduction of $\kappa_l$ upon the introduction of micro/nano structural defects. The lines show the $\kappa_l = Av_s^3T^{-1}$ model describing phonon thermal conductivity in the high-T limit where the only scattering mechanism is phonon-phonon scattering. A is normalized to the Na-PbTe sample and fixed. The shaded region shows the reduction in $\kappa_l$ expected from lattice softening alone, without assuming an increase in phonon-defect scattering centers. Phonon scattering mechanisms could account for the remaining reduction in $\kappa_l$, depicted by the cross-hatched region. The speed of sound ($v_s$) reduction, measured in this study, is given in the legend. The circles are data for a Na-doped (0.75% Na) sample synthesized and measured in this study. The square data points are a low dislocation density sample from reference ($Na_{0.015}Eu_{0.03}Pb_{0.955}Te$). Copyright 2019, Wiley[28]; (F) Lattice thermal conductivity versus temperature under different biaxial tensile strains (δ = 0%, 2%, 4%, 6%, and 8%) of unstrained and strained 1T-SnSSe monolayers. Copyright 2022, Elsevier[92]; Phonon dispersion relations for (G) Mg2Si; (H) $Mg_2Si_{0.375}Sn_{0.625}$; and (I) $Mg_2Sn$; the gradually changing colors indicate the group velocity for the corresponding phonon branches; (J) shows their acoustic phonon branches along the "Γ-X" direction. Copyright 2017, AIP Publishing[99]. FWHM: Full width at half maximum.

## Thermal expansion coefficient

The thermal expansion coefficient[100-103] is a physical quantity related to the size of materials, which describes the volume change degree of the material when the temperature changes [Figure 7A]. Lattice

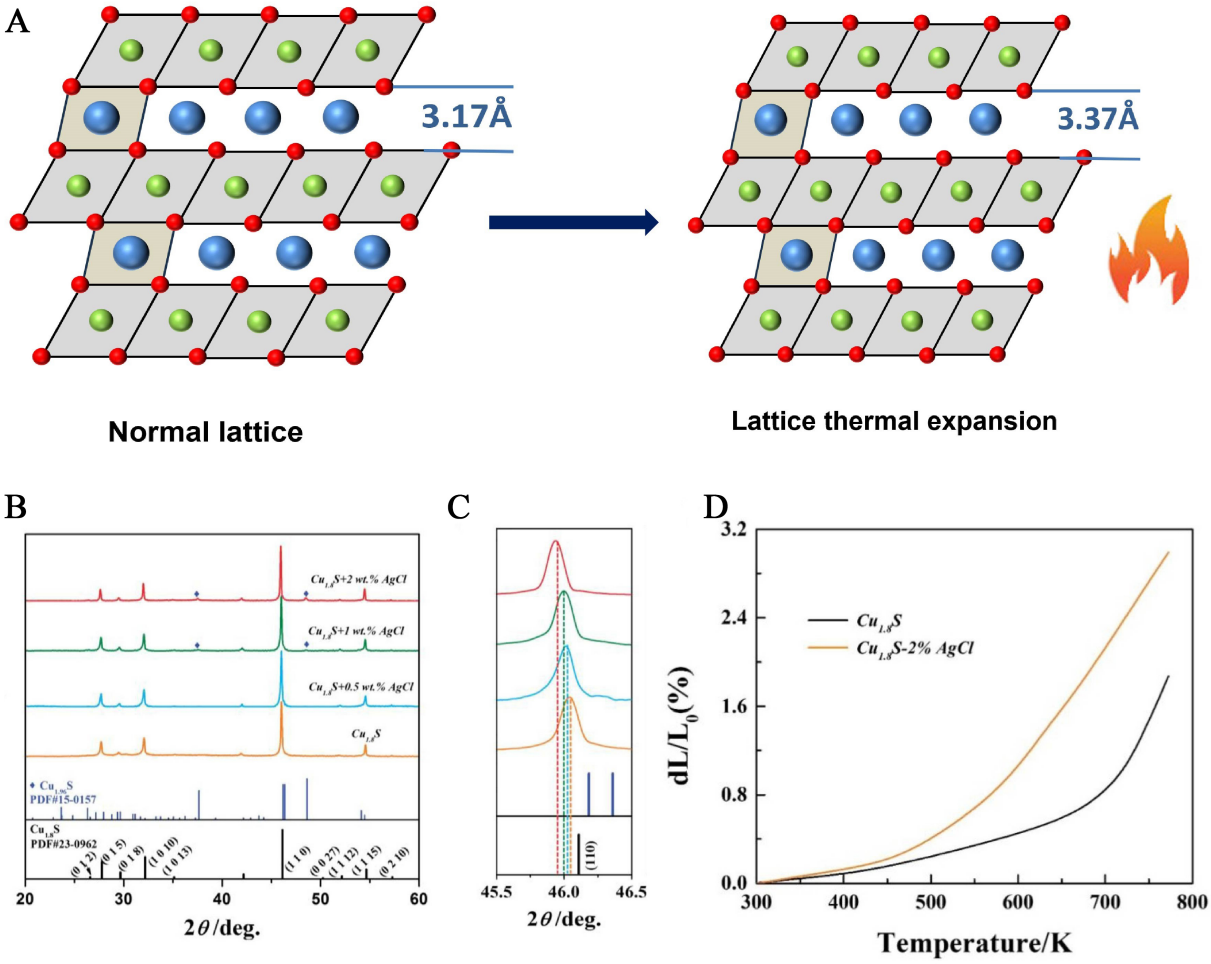


**Figure 7.** (A) Diagram of the effect of lattice softening on the coefficient of thermal expansion; (B) The XRD patterns of SPS-treated $Cu_{1.8}$S-x% AgCl bulk specimens with different x values; (C) The enlarged patterns between 45.5° to 46.5° and the relative mass density of the samples; (D) The thermal expansion rate of $Cu_{1.8}$S and $Cu_{1.8}$S-2% AgCl in 300 K to 773 K. Copyright 2021, Elsevier[104]. SPS: Spark plasma sintering; XRD: X-ray diffraction.

softening may directly or indirectly affect the thermal expansion behavior of materials through a variety of mechanisms. These mechanisms include increased phonon scattering, enhanced anharmonic effects, changes in the Grüneisen constant, modifications of material properties, and the influence of carrier dynamics.

Zhang *et al.*[104] investigated the effects of introducing AgCl into $Cu_{1.8}$S. With the addition of AgCl, the (110) diffraction peak of $Cu_{1.8}$S moves to the left [Figure 7B and C]. This is because the larger $Ag^+$(1.15 Å) replaces the site of $Cu^+$(0.96 Å), resulting in an increase in lattice volume. The change of lattice volume is an external manifestation of lattice softening, indicating that the distance and interaction between atoms have changed, reducing the rigidity of the lattice, making it more prone to deformation, and thus reflecting the trend of lattice softening. Lattice softening also increases the thermal expansion rate of $Cu_{1.8}$S, and the thermal expansion rate $dL/L_0$ of the $Cu_{1.8}$S-1% AgCl sample increases rapidly after 500 K [Figure 7D], which is due to the more serious volatilization of sulfur after the introduction of AgCl and the damage of chemical bond strength.

In the field of material design, the thermal expansion coefficient is of great significance. By controlling the thermal expansion coefficient of the material, the thermal stress can be effectively reduced and the temperature stability and reliability of the material can be improved.

## CONCLUSION AND OUTLOOK

Lattice softening offers a universal way to optimize thermoelectric properties through material design. In this paper, we first conclude three ways to achieve lattice softening, including mechanical strain engineering, chemical doping, and phase transition, and then discuss their distinct softening mechanisms by showing related examples. In addition, the effects of lattice softening on the electrical and thermal transport properties of TE materials are summarized. We believe that the continuous development and improvement of lattice softening technology will provide strong support for the design and preparation of high-performance thermoelectric materials, and promote the wide application of thermoelectric technology in the fields of energy recovery, temperature difference power generation, and thermal management.

In the future, with the continuous deepening of research and technological progress, lattice softening is expected to make breakthroughs in many aspects. First, through precise strain engineering and chemical doping, the lattice structure of the material can be more precisely regulated, which may further reduce the thermal conductivity and increase the conductivity and Seebeck coefficient, significantly improving the *ZT* value. Secondly, by introducing nanoparticles and nanocomposite structures, not only can the flexibility of the lattice be optimized, but also the phonon scattering can be more effectively increased, leading to improved thermoelectric conversion efficiency of the material. In addition, combined with advanced characterization techniques such as in situ extended X-ray absorption fine structure (EXAFS), *in situ* transmission electron microscopy (TEM), and inelastic neutron scattering, a deeper understanding of the effect of lattice softening on the microstructure of materials can be achieved, enabling finer regulation. Finally, more novel lattice softening methods can be developed to expand their applications in semiconductor, optical and magnetic materials through interdisciplinary cooperation.

## DECLARATIONS

### Authors' contributions

Design and conception of the study, literature search, reference organization, data collection, data analysis, and manuscript drafting: Li, C.; Zhou, Z.

Provision of technical and material support, scientific discussion consultation, and manuscript revision suggestions: Fu, L.; Lou, Y.

All authors participated in the composition of the manuscript.

### Availability of data and materials

Not applicable.

### Financial support and sponsorship

None.

### Conflicts of interest

All authors declared that there are no conflicts of interest.

### Ethical approval and consent to participate

Not applicable.

## Consent for publication

Not applicable.

## Copyright



## REFERENCES


1. Tan, Z.; Feng, X.; Yang, M.; Wang, Y. Energy and economic performance comparison of heat pump and power cycle in low grade waste heat recovery. *Energy* **2022**, *260*, 125149. DOI
2. Lu, X.; Pan, G.; Shi, Z.; Xu, B.; Lou, Y. Recent advances in interface engineering of thermoelectric nanomaterials. *Mater. Chem. Front.* **2023**, *7*, 4707-22. DOI
3. Chen, Y.; Hong, G.; Li, L.; et al. Enlightening thermoelectric mastery: bio-inspired cellulose gel containing eco-friendly deep eutectic solvents. *Chem. Eng. J.* **2024**, *483*, 149344. DOI
4. Miao, L.; Zhu, S.; Liu, C.; et al. Comfortable wearable thermoelectric generator with high output power. *Nat. Commun.* **2024**, *15*, 8516. DOI PubMed PMC
5. Beretta, D.; Perego, A.; Lanzani, G.; Caironi, M. Organic flexible thermoelectric generators: from modeling, a roadmap towards applications. *Sustain. Energy. Fuels.* **2017**, *1*, 174-90. DOI
6. Yang, S. E.; Han, H.; Son, J. S. Recent progress in 3D printing of $Bi_2Te_3$-based thermoelectric materials and devices. *J. Phys. Energy.* **2024**, *6*, 022003. DOI
7. Muddasar, M.; Menéndez, N.; Quero, Á.; et al. Highly-efficient sustainable ionic thermoelectric materials using lignin-derived hydrogels. *Adv. Compos. Hybrid. Mater.* **2024**, *7*, 863. DOI
8. Li, C.; Jiang, F.; Liu, C.; Liu, P.; Xu, J. Present and future thermoelectric materials toward wearable energy harvesting. *Appl. Mater. Today.* **2019**, *15*, 543-57. DOI
9. Du, K.; Wu, C. An innovative tubular thermoelectric generator (TTEG) for enhanced waste heat recovery in industrial and automotive applications. *Appl. Sci.* **2024**, *14*, 685. DOI
10. Wang, J.; Chen, Y.; Liu, Y.; Liu, G.; Cai, R. Harvesting waste heat based on thermoelectric generation to drive LED car lamps. *J. Therm. Anal. Calorim.* **2024**, *149*, 3427-42. DOI
11. Su, H.; Lin, P.; Lu, H.; Chen, Y. Efficient solar-thermal conversion and thermal energy storage towards personal thermal management and thermoelectric power generation enabled by massive screen printing of carbon nanotube dopped energy storage gels. *J. Energy. Storage.* **2024**, *76*, 109782. DOI
12. Lewis, N. S. Research opportunities to advance solar energy utilization. *Science* **2016**, *351*, aad1920. DOI PubMed
13. Chen, C.; Xu, F. Q.; Wu, Y.; et al. Manipulating hetero-nanowire films for flexible and multifunctional thermoelectric devices. *Adv. Mater.* **2024**, *36*, e2400020. DOI
14. Han, Y.; Wei, H.; Du, Y.; et al. Ultrasensitive flexible thermal sensor arrays based on high-thermopower ionic thermoelectric hydrogel. *Adv. Sci. (Weinh).* **2023**, *10*, e2302685. DOI PubMed PMC
15. Gu, H.; Kang, S.; Fu, Y.; et al. High seebeck coefficient inorganic $Ge_{15}Ga_{10}Te_{75}$ core/polymer cladding fibers for respiration and body temperature monitoring. *ACS. Appl. Mater. Interfaces.* **2023**, *15*, 59768-75. DOI
16. Gupta, A.; Agrawal, S.; Pal, Y. Effect of thermoelectric materials in electrical and thermal performance of photovoltaic thermal (PVT) collector. *IOP. Conf. Ser:. Mater. Sci. Eng.* **2019**, *691*, 012036. DOI
17. Zhang, Y.; Wang, W.; Zhang, F.; et al. Soft organic thermoelectric materials: principles, current state of the art and applications. *Small* **2022**, *18*, e2104922. DOI
18. Shi, X. L.; Zou, J.; Chen, Z. G. Advanced thermoelectric design: from materials and structures to devices. *Chem. Rev.* **2020**, *120*, 7399-515. DOI PubMed
19. He, J.; Xu, J.; Tan, X.; et al. Synthesis of SnTe/$AgSbSe_2$ nanocomposite as a promising lead-free thermoelectric material. *J. Materiomics.* **2016**, *2*, 165-71. DOI
20. Zhang, C.; de, M. M.; Li, Z.; et al. Enhanced thermoelectric performance of solution-derived bismuth telluride based nanocomposites via liquid-phase Sintering. *Nano. Energy.* **2016**, *30*, 630-8. DOI
21. Chen, Y.; Nisar, M.; Qin, W.; et al. Integration of boron nitride into tin-enriched $SnSe_2$ for a high-performance thermoelectric nanocomposite with optimized electrical transport and mechanical properties. *Adv. Funct. Mater.* **2025**, 202425050. DOI
22. Liu, W.; Yin, L.; Li, L.; et al. Grain boundary re-crystallization and sub-nano regions leading to high plateau figure of merit for $Bi_2Te_3$ nanoflakes. *Energy. Environ. Sci.* **2023**, *16*, 5123-35. DOI
23. Gordillo, J. M.; Morata, A.; Sierra, C. D.; Salleras, M.; Fonseca, L.; Tarancón, A. Recent advances in silicon-based nanostructures for thermoelectric applications. *APL. Materials.* **2023**, *11*, 040702. DOI
24. Yao, G.; Chen, Y.; Wang, S.; et al. Boosting thermoelectric performance of $PbBi_2Te_4$ via reduced carrier scattering and intensified phonon scattering. *Small* **2024**, *20*, e2400449. DOI
25. Tan, X.; Wang, L.; Shao, H.; et al. Improving thermoelectric performance of α-mgagsb by theoretical band engineering design. *Adv. Energy. Mater.* **2017**, *7*, 1700076. DOI

26. Yu, L.; Wei, S. T.; Wang, L. J.; et al. Band engineering and phonon engineering Effectively improve n-type $Mg_3Sb_2$ thermoelectric material properties. *ACS. Appl. Mater. Interfaces.* **2023**, *15*, 53594-603. DOI
27. Slade, T. J.; Anand, S.; Wood, M.; et al. Charge-carrier-mediated lattice softening contributes to high zT in thermoelectric semiconductors. *Joule* **2021**, *5*, 1168-82. DOI
28. Hanus, R.; Agne, M. T.; Rettie, A. J. E.; et al. Lattice softening significantly reduces thermal conductivity and leads to high thermoelectric efficiency. *Adv. Mater.* **2019**, *31*, e1900108. DOI
29. Tan, G.; Hao, S.; Hanus, R. C.; et al. High thermoelectric performance in SnTe-$AgSbTe_2$ alloys from lattice softening, giant phonon-vacancy scattering, and valence band convergence. *ACS. Energy. Lett.* **2018**, *3*, 705-12. DOI
30. Muchtar, A. R.; Srinivasan, B.; Tonquesse, S. L.; et al. Physical insights on the lattice softening driven mid-temperature range thermoelectrics of Ti/Zr-inserted SnTe - an outlook beyond the horizons of conventional phonon scattering and excavation of heikes' equation for estimating carrier properties. *Adv. Energy. Mater.* **2021**, *11*, 2101122. DOI
31. Liu, M.; Guo, M.; Zhu, J.; et al. High-performance $CaMg_2Bi_2$-based thermoelectric materials driven by lattice softening and orbital alignment via cadmium doping. *Adv. Funct. Mater.* **2024**, *34*, 2316075. DOI
32. Shen, X.; Zhang, B.; Chen, Q.; et al. Synergistically optimized thermoelectric properties of $Ag_{1+x}In_5Se_8$ alloys. *Inorg. Chem. Front.* **2019**, *6*, 3545-53. DOI
33. Zhong, J.; Yang, X.; Lyu, T.; et al. Nuanced dilute doping strategy enables high-performance GeTe thermoelectrics. *Sci. Bull. (Beijing).* **2024**, *69*, 1037-49. DOI
34. Tippireddy, S.; Azough, F.; Vikram; et al. Local structural distortions and reduced thermal conductivity in Ge-substituted chalcopyrite. *J. Mater. Chem. A.* **2022**, *10*, 23874-85. DOI
35. Parashchuk, T.; Wiendlocha, B.; Cherniushok, O.; Knura, R.; Wojciechowski, K. T. High thermoelectric performance of p-type PbTe enabled by the synergy of resonance scattering and lattice softening. *ACS. Appl. Mater. Interfaces.* **2021**, *13*, 49027-42. DOI PubMed
36. Chen, Y.; Fu, Z.; Wu, Y.; et al. Giant heterogeneous magnetostriction induced by charge accumulation-mediated nanoinclusion formation in dual-phase nanostructured systems. *Acta. Materialia.* **2021**, *213*, 116975. DOI
37. Guan, C.; Chen, B.; Jiang, L.; et al. Atomic-scale insights into ω-variants in Galfenol triggered by displacive-diffusive transformation. *Mater. Design.* **2021**, *205*, 109745. DOI
38. Rahman, N.; Gou, J.; Liu, X.; Ma, T.; Yan, M. Enhanced magnetostriction of $Fe_{81}Ga_{19}$ by approaching an instable phase boundary. *Scripta. Materialia.* **2018**, *146*, 200-3. DOI
39. Guo, S.; Li, H.; Lu, Y.; Liu, Z.; Hu, X. Lattice softening enables highly reversible sodium storage in anti-pulverization Bi-Sb alloy/carbon nanofibers. *Energy. Storage. Mater.* **2020**, *27*, 270-8. DOI
40. Mizoguchi, H.; Park, S. W.; Hosono, H. A view on formation gap in transition metal hydrides and its collapse. *J. Am. Chem. Soc.* **2021**, *143*, 11345-8. DOI PubMed
41. Yang, J.; Zhang, X.; Ge, B.; et al. Effect of Zn migration on the thermoelectric properties of $Zn_4Sb_3$ material. *Ceram. Int.* **2017**, *43*, 15275-80. DOI
42. Zhang, D.; He, P.; Liu, G.; et al. High thermoelectric performance of PbSe via a synergistic band engineering and dislocation approach. *Scripta. Materialia.* **2024**, *244*, 116003. DOI
43. Bai, Y.; Li, X.; Ouyang, T.; et al. High thermoelectric performance in the n-type $Bi_2S_3$/f-MWCNTs nanocomposites prepared by hydrothermal method. *Carbon* **2023**, *212*, 118158. DOI
44. Lv, H. Y.; Lu, W. J.; Shao, D. F.; Lu, H. Y.; Sun, Y. P. Strain-induced enhancement in the thermoelectric performance of a $ZrS_2$ monolayer. *J. Mater. Chem. C.* **2016**, *4*, 4538-45. DOI
45. Guo, Z.; Wang, J.; Yin, W. Atomistic origin of lattice softness and its impact on structural and carrier dynamics in three dimensional perovskites. *Energy. Environ. Sci.* **2022**, *15*, 660-71. DOI
46. Zhang, G.; Zhang, Y. Strain effects on thermoelectric properties of two-dimensional materials. *Mech. Mater.* **2015**, *91*, 382-98. DOI
47. Wu, Y.; Chen, Z.; Nan, P.; et al. Lattice strain advances thermoelectrics. *Joule* **2019**, *3*, 1276-88. DOI
48. Sprague, L. W.; Huang, C.; Song, J.; Rubenstein, B. M. Maximizing thermoelectric figures of merit by uniaxially straining indium selenide. *J. Phys. Chem. C.* **2019**, *123*, 25437-47. DOI
49. Yu, C.; Zhang, G.; Zhang, Y.; Peng, L. Strain engineering on the thermal conductivity and heat flux of thermoelectric $Bi_2Te_3$ nanofilm. *Nano. Energy.* **2015**, *17*, 104-10. DOI
50. Song, X.; Wang, G.; Gan, S.; et al. Triaxial strain enhanced thermoelectric performance and conversion efficiency in $Tl_3TaSe_4$. *J. Alloys. Compd.* **2024**, *1004*, 175896. DOI
51. Huang, M.; Yan, H.; Chen, C.; Song, D.; Heinz, T. F.; Hone, J. Phonon softening and crystallographic orientation of strained graphene studied by Raman spectroscopy. *Proc. Natl. Acad. Sci. U. S. A.* **2009**, *106*, 7304-8. DOI PubMed PMC
52. Xu, B.; Liao, Y.; Fang, Z.; et al. Extremely suppressed thermal conductivity of large-scale nanocrystalline silicon through inhomogeneous internal strain engineering. *J. Mater. Chem. A.* **2023**, *11*, 19017-24. DOI
53. Moure, A.; Rull-bravo, M.; Abad, B.; et al. Thermoelectric skutterudite/oxide nanocomposites: effective decoupling of electrical and thermal conductivity by functional interfaces. *Nano. Energy.* **2017**, *31*, 393-402. DOI
54. Mustafa, G.; Minhas, N.; Singh, H.; et al. Lattice softness regulates recombination and lifetime of carrier in Germanium doped $CsPbI_2$ Br perovskite: first principles DFT and NAMD simulations. *J. Solid. State. Chem.* **2023**, *322*, 123981. DOI
55. Lee, S.; Esfarjani, K.; Luo, T.; Zhou, J.; Tian, Z.; Chen, G. Resonant bonding leads to low lattice thermal conductivity. *Nat. Commun.*

**2014**, *5*, 3525. DOI
56. Hu, J.; Zhu, J.; Dong, X.; et al. Breaking the minimum limit of thermal conductivity of $Mg_3Sb_2$ thermoelectric mediated by chemical alloying induced lattice instability. *Small* **2023**, *19*, e2301382. DOI
57. Back, S. Y.; Cho, H.; Kim, Y.; et al. Enhancement of thermoelectric properties by lattice softening and energy band gap control in Te-deficient $InTe_{1-\delta}$. *AIP. Advances.* **2018**, *8*, 115227. DOI
58. Zhang, Y.; Li, Y.; Mao, W.; Zhang, X.; Zhang, J.; Luo, J. Balancing structural stability and thermoelectric performance of $GeMnTe_2$ by manipulating the complexity of cation sublattice. *Mater. Today. Phys.* **2025**, *52*, 101693. DOI
59. Zhang, C.; Jin, K.; Dong, H.; et al. Synergistic enhancement of thermoelectric performance of n-type PbTe by resonant level and single-atom-layer vacancies. *Nano. Energy.* **2024**, *126*, 109615. DOI
60. Zhu, H.; Zhao, C.; Nan, P.; et al. intrinsically low lattice thermal conductivity in natural superlattice $(Bi_2)m(Bi_2Te_3)n$ thermoelectric materials. *Chem. Mater.* **2021**, *33*, 1140-8. DOI
61. Yang, W. J.; Ha, T.; Park, B. C.; et al. Switching to hidden metallic crystal phase in phase-change materials by photoenhanced metavalent bonding. *ACS. Nano.* **2022**, *16*, 2024-31. DOI
62. Zhang, W.; Zhang, H.; Sun, S.; et al. Metavalent bonding in layered phase-change memory materials. *Adv. Sci.* **2023**, *10*, 2370094. DOI PMC
63. Guarneri, L.; Jakobs, S.; von, H. A.; et al. Metavalent bonding in crystalline solids: how does it collapse? *Adv. Mater.* **2021**, *33*, e2102356. DOI PubMed PMC
64. Sarkar, D.; Roychowdhury, S.; Arora, R.; et al. Metavalent bonding in gese leads to high thermoelectric performance. *Angew. Chem. Int. Ed. Engl.* **2021**, *60*, 10350-8. DOI
65. Pathak, R.; Joseph, A.; Dutta, P.; et al. Impact of pressure on metavalent bonding in bite influencing electronic topological transitions. *Angew. Chem. Int. Ed. Engl.* **2025**, *64*, e202422652. DOI
66. Liu, Y.; Zhang, X.; Nan, P.; et al. Improved solubility in metavalently bonded solid leads to band alignment, ultralow thermal conductivity, and high thermoelectric performance in SnTe. *Adv. Funct. Mater.* **2022**, *32*, 2209980. DOI
67. Wang, Y.; Long, Z.; Cheng, Y.; et al. Chemical bonding engineering for high-symmetry $Cu_2S$-based materials with high thermoelectric performance. *Mater. Today. Phys.* **2023**, *32*, 101028. DOI
68. Zhu, T.; Su, X.; Zhang, Q.; Tang, X. Structural transformation and thermoelectric performance in $Ag_2Te_{1-x}Se_x$ solid solution. *J. Alloys. Compd.* **2021**, *871*, 159507. DOI
69. Rundle, J.; Leoni, S. Layered tin chalcogenides SnS and SnSe: lattice thermal conductivity benchmarks and thermoelectric figure of merit. *J. Phys. Chem. C. Nanomater. Interfaces.* **2022**, *126*, 14036-46. DOI PubMed PMC
70. Guo, F.; Liu, M.; Zhu, J.; et al. Suppressing lone-pair expression endows room-temperature cubic structure and high thermoelectric performance in GeTe-based materials. *Mater. Today. Phys.* **2022**, *27*, 100780. DOI
71. Shrestha, R.; Luan, Y.; Shin, S.; et al. High-contrast and reversible polymer thermal regulator by structural phase transition. *Sci. Adv.* **2019**, *5*, eaax3777. DOI PubMed PMC
72. Wang, Y.; Xiao, J.; Zhu, H.; et al. Structural phase transition in monolayer $MoTe_2$ driven by electrostatic doping. *Nature* **2017**, *550*, 487-91. DOI
73. Migliorini, A.; Kuerbanjiang, B.; Huminiuc, T.; et al. Spontaneous exchange bias formation driven by a structural phase transition in the antiferromagnetic material. *Nat. Mater.* **2018**, *17*, 28-35. DOI
74. Xiao, C.; Xu, J.; Li, K.; Feng, J.; Yang, J.; Xie, Y. Superionic phase transition in silver chalcogenide nanocrystals realizing optimized thermoelectric performance. *J. Am. Chem. Soc.* **2012**, *134*, 4287-93. DOI
75. Singh, B.; Gupta, M. K.; Mittal, R.; Chaplot, S. L. *Ab initio* molecular dynamics study of 1-D superionic conduction and phase transition in β-eucryptite. *J. Mater. Chem. A.* **2018**, *6*, 5052-64. DOI
76. Lee, S.; Lin, Z.; Huang, J.; et al. Programmable devices based on reversible solid-state doping of two-dimensional semiconductors with superionic silver iodide. *Nat. Electron.* **2020**, *3*, 630-7. DOI
77. Ruta, F. L.; Kim, B. S. Y.; Sun, Z.; et al. Surface plasmons induce topological transition in graphene/α-$MoO_3$ heterostructures. *Nat. Commun.* **2022**, *13*, 3719. DOI PubMed PMC
78. Xie, Y.; Wang, C.; Fei, F.; et al. Tunable optical topological transitions of plasmon polaritons in $WTe_2$ van der Waals films. *Light. Sci. Appl.* **2023**, *12*, 193. DOI PubMed PMC
79. Sinha, S.; Adak, P. C.; Chakraborty, A.; et al. Berry curvature dipole senses topological transition in a moiré superlattice. *Nat. Phys.* **2022**, *18*, 765-70. DOI
80. Shen, X.; Heid, R.; Hott, R.; et al. Precursor region with full phonon softening above the charge-density-wave phase transition in 2*H*-$TaSe_2$. *Nat. Commun.* **2023**, *14*, 7282. DOI PubMed PMC
81. Wang, S.; Sun, Y.; Yang, J.; et al. High thermoelectric performance in Te-free $(Bi,Sb)_2Se_3$ via structural transition induced band convergence and chemical bond softening. *Energy. Environ. Sci.* **2016**, *9*, 3436-47. DOI
82. Yang, S.; Lin, C.; He, X.; et al. Unlocking ultralow thermal conductivity in α-CuTeI via specific symmetry breaking in Cu sublattice. *Adv. Funct. Mater.* **2025**, *35*, 2419776. DOI
83. Guin, S. N.; Sanyal, D.; Biswas, K. The effect of order-disorder phase transitions and band gap evolution on the thermoelectric properties of AgCuS nanocrystals. *Chem. Sci.* **2016**, *7*, 534-43. DOI PubMed PMC
84. Shen, X.; Koza, M. M.; Tung, Y. H.; et al. Soft phonon mode triggering fast Ag diffusion in superionic argyrodite $Ag_8GeSe_6$. *Small* **2023**, *19*, e2305048. DOI

85. Beaulieu, S.; Dong, S.; Tancogne-Dejean, N.; et al. Ultrafast dynamical Lifshitz transition. *Sci. Adv.* **2021**, *7*, eabd9275. DOI PubMed PMC
86. Jung, H.; Jin, K. H.; Sung, M.; Kim, J.; Kim, J.; Yeom, H. W. Quantum-confined lifshitz transition on weyl semimetal $T_d$-$MoTe_2$. *ACS. Nano.* **2024**, *18*, 23189-95. DOI PubMed PMC
87. Chi, Z.; Zhang, J.; Gong, Z.; et al. Pressure-induced Lifshitz transition in the type-II Weyl semimetal WP2. *Mater. Today. Phys.* **2024**, *42*, 101372. DOI
88. Wu, W.; Shi, Z.; Du, Y.; et al. Topological Lifshitz transition and one-dimensional Weyl mode in $HfTe_5$. *Nat. Mater.* **2023**, *22*, 84-91. DOI
89. Noad, H. M. L.; Ishida, K.; Li, Y. S.; et al. Giant lattice softening at a Lifshitz transition in $Sr_2RuO_4$. *Science* **2023**, *382*, 447-50. DOI
90. Zhang, D.; Yang, J.; Bai, H.; et al. Significant average *ZT* enhancement in $Cu_3SbSe_4$-based thermoelectric material *via* softening p-d hybridization. *J. Mater. Chem. A.* **2019**, *7*, 17648-54. DOI
91. Liang, J.; Yang, H.; Liu, C.; et al. Realizing a high ZT of 1.6 in N-type $Mg_3Sb_2$-based Zintl compounds through Mn and Se codoping. *ACS. Appl. Mater. Interfaces.* **2020**, *12*, 21799-807. DOI
92. Tang, S.; Bai, S.; Wu, M.; et al. Improving thermoelectric performance of asymmetrical Janus 1T-SnSSe monolayer by the synergistic effect of band convergence and crystal lattice softening under strain engineering. *Mater. Today. Phys.* **2022**, *29*, 100923. DOI
93. Kim, H.; Park, G.; Park, S.; Kim, W. Strategies for manipulating phonon transport in solids. *ACS. Nano.* **2021**, *15*, 2182-96. DOI
94. Zhao, Y.; Zhang, G.; Nai, M. H.; et al. Probing the physical origin of anisotropic thermal transport in black phosphorus nanoribbons. *Adv. Mater.* **2018**, *30*, e1804928. DOI
95. Zhao, Y.; Yang, L.; Kong, L.; et al. Ultralow thermal conductivity of single-crystalline porous silicon nanowires. *Adv. Funct. Mater.* **2017**, *27*, 1702824. DOI
96. Cappai, A.; Melis, C.; Marongiu, D.; et al. Strong anharmonicity at the origin of anomalous thermal conductivity in double perovskite $Cs_2NaYbCl_6$. *Adv. Sci. (Weinh).* **2024**, *11*, e2305861. DOI PubMed PMC
97. Jiang, B.; Wang, W.; Liu, S.; et al. High figure-of-merit and power generation in high-entropy GeTe-based thermoelectrics. *Science* **2022**, *377*, 208-13. DOI
98. Han, S.; Dai, S.; Ma, J.; et al. Strong phonon softening and avoided crossing in aliovalence-doped heavy-band thermoelectrics. *Nat. Phys.* **2023**, *19*, 1649-57. DOI
99. Tan, X. J.; Liu, G. Q.; Shao, H. Z.; et al. Acoustic phonon softening and reduced thermal conductivity in $Mg2Si_{1-x}$ $Sn_x$ solid solutions. *Appl. Phys. Lett.* **2017**, *110*, 143903. DOI
100. Chen, Z.; Tian, Z.; Zheng, L.; et al. $(Ho_{0.25}Lu_{0.25}Yb_{0.25}Eu_{0.25})_2SiO_5$ high-entropy ceramic with low thermal conductivity, tunable thermal expansion coefficient, and excellent resistance to CMAS corrosion. *J. Adv. Ceram.* **2022**, *11*, 1279-93. DOI
101. Kucinski, T. M.; Dhall, R.; Savitzky, B. H.; et al. Direct measurement of the thermal expansion coefficient of epitaxial $WSe_2$ by four-dimensional scanning transmission electron microscopy. *ACS. Nano.* **2024**, *18*, 17725-34. DOI PubMed PMC
102. Onodera, Y.; Kohara, S.; Masai, H.; Koreeda, A.; Okamura, S.; Ohkubo, T. Formation of metallic cation-oxygen network for anomalous thermal expansion coefficients in binary phosphate glass. *Nat. Commun.* **2017**, *8*, 15449. DOI PubMed PMC
103. Kano, E.; Malac, M.; Hayashida, M. Substrate and contamination effects on the thermal expansion coefficient of suspended graphene measured by electron diffraction. *Carbon* **2020**, *163*, 324-32. DOI
104. Zhang, Y.; Feng, J.; Ge, Z. Enhanced thermoelectric performance of $Cu_{1.8}S$ via lattice softening. *Chem. Eng. J.* **2022**, *428*, 131153. DOI